Bioactive Materials 36 (2024) 48–61

Contents lists available at ScienceDirect

Bioactive Materials

journal homepage: www.keaipublishing.com/en/journals/bioactive-materials

Tailoring therapeutics via a systematic beneficial elements comparison between photosynthetic bacteria-derived OMVs and extruded nanovesicles

Tingshan Xiao [a,c], Yichuan Ma [c,d], Ziyang Zhang [a,c], Yixin Zhang [a,c], Yu Zhao [a,c], Xiaohan Zhou [b], Xueyi Wang [b], Kun Ge [c,d], Junshu Guo [b], Jinchao Zhang [c,d,***], Zhenhua Li [b,**], Huifang Liu [a,c,*]

[a] College of Pharmaceutical Science, Key Laboratory of Pharmaceutical Quality Control of Hebei Province, Hebei University, Baoding, 071002, China
[b] The Tenth Affiliated Hospital, Southern Medical University (Dongguan People's Hospital), Guangdong Provincial Key Laboratory of Cardiac Function and Microcirculation, Dongguan 523000, China
[c] State Key Laboratory of New Pharmaceutical Preparations and Excipients, Key Laboratory of Medicinal Chemistry and Molecular Diagnosis of Ministry of Education, Chemical Biology Key Laboratory of Hebei Province, Hebei University, Baoding, 071002, China
[d] College of Chemistry & Materials Science, Hebei University, Baoding, 071002, China

ARTICLE INFO

Keywords:
Photosynthetic bacteria
Outer membrane vesicles
Bacteria-derived nanovesicles
Antitumor
Lysophosphatidylcholine

ABSTRACT

Photosynthetic bacteria (PSB) has shown significant potential as a drug or drug delivery system owing to their photothermal capabilities and antioxidant properties. Nevertheless, the actualization of their potential is impeded by inherent constraints, including their considerable size, heightened immunogenicity and compromised biosafety. Conquering these obstacles and pursuing more effective solutions remains a top priority. Similar to extracellular vesicles, bacterial outer membrane vesicles (OMVs) have demonstrated a great potential in biomedical applications. OMVs from PSB encapsulate a rich array of bioactive constituents, including proteins, nucleic acids, and lipids inherited from their parent cells. Consequently, they emerge as a promising and practical alternative. Unfortunately, OMVs have suffered from low yield and inconsistent particle sizes. In response, bacteria-derived nanovesicles (BNVs), created through controlled extrusion, adeptly overcome the challenges associated with OMVs. However, the differences, both in composition and subsequent biological effects, between OMVs and BNVs remain enigmatic. In a groundbreaking endeavor, our study meticulously cultivates PSB-derived OMVs and BNVs, dissecting their nuances. Despite minimal differences in morphology and size between PSB-derived OMVs and BNVs, the latter contains a higher concentration of active ingredients and metabolites. Particularly noteworthy is the elevated levels of lysophosphatidylcholine (LPC) found in BNVs, known for its ability to enhance cell proliferation and initiate downstream signaling pathways that promote angiogenesis and epithelialization. Importantly, our results indicate that BNVs can accelerate wound closure more effectively by orchestrating a harmonious balance of cell proliferation and migration within NIH-3T3 cells, while also activating the EGFR/AKT/PI3K pathway. In contrast, OMVs have a pronounced aptitude in anti-cancer efforts, driving macrophages toward the M1 phenotype and promoting the release of inflammatory cytokines. Thus, our findings not only provide a promising methodological framework but also establish a definitive criterion for discerning the optimal application of OMVs and BNVs in addressing a wide range of medical conditions.

Peer review under responsibility of KeAi Communications Co., Ltd.

* Corresponding author. College of Pharmaceutical Science, Key Laboratory of Pharmaceutical Quality Control of Hebei Province, Hebei University, Baoding, 071002, China.

** Corresponding author. The Tenth Affiliated Hospital, Southern Medical University (Dongguan People's Hospital), Guangdong Provincial Key Laboratory of Cardiac Function and Microcirculation, Dongguan 523000, China.

*** Corresponding author. State Key Laboratory of New Pharmaceutical Preparations and Excipients, Key Laboratory of Medicinal Chemistry and Molecular Diagnosis of Ministry of Education, Chemical Biology Key Laboratory of Hebei Province, Hebei University, Baoding, 071002, China.

E-mail addresses: jczhang6970@163.com (J. Zhang), zhenhuali@hbu.edu.cn (Z. Li), liuhuifang@hbu.edu.cn (H. Liu).

https://doi.org/10.1016/j.bioactmat.2024.02.025
Received 16 November 2023; Received in revised form 19 February 2024; Accepted 20 February 2024

1. Introduction

Photosynthetic bacteria (PSB) belong to the category of facultative anaerobic bacteria and possess the capability to engage in photosynthesis [1,2]. In previous efforts, we established non-toxic and non-pathogenic platforms utilizing PSB for cancer therapy and wound healing. These platforms leverage the anaerobic characteristics, near-infrared phototactic properties, and photothermal effects of PSB [3–8]. Although promising, however, the application of live PSB still present certain limitations. Notably, concerns revolve around the potential unchecked proliferation of live bacteria within the body, prompting valid safety considerations [9]. Additionally, the elongated morphology of PSB, with a length of approximately 2 μm, poses challenges for intravenous administration due to its micro-scale proportions [10]. Moreover, even in cases of localized delivery, the sizable dimensions of these bacteria hinder their infiltration into densely packed solid tumors. As a result, the exploration of an alternative bacterial therapy strategy emerges as an imperative pursuit.

Outer membrane vesicles (OMVs) are diminutive, spherical structures that are naturally produced by gram-negative bacteria [11]. OMVs contain abundant pathogen-associated molecular patterns (PAMPs), including lipopolysaccharides (LPS), peptidoglycan (PG), DNA, RNA, etc. It can be recognized by the host cell's pattern recognition receptors, activating its natural immune response and anti-inflammatory properties [12]. As such, OMVs unfolds a new territory for bacteria alternative therapy and gains increasing attention in recent years. Much akin to their extracellular counterparts (EVs), OMVs have been used as natural nanocarriers for delivering drugs, vaccines, and other therapeutic agents [13–15]. However, both the poor yield rate and batch-to-batch stability of OMVs present a significant barrier for clinical translation and large-scale manufacture [15–17]. The emergence of the mechanical cell extrusion method has effectively solved the problems. Swiftly, this method has unfurled a tapestry where an abundance of nanovesicles (NVs) can be summoned into existence in mere moments. In 2013, Jang et al. first reported the use of a mechanical extrusion method to produce NVs of copious yield, unwavering stability and purity [18]. Compared to naturally secreted EVs, these NVs march forth with augmented productivity, thereby shearing the cost veil that shrouds large-scale production. Currently, research on bacterial nanovesicles (BNVs) mainly focused on *Escherichia coli* and only investigate their morphology and size, followed by verification of their biological functions [19,20]. Numerous studies employ NVs as a direct substitute for EVs, yet inherent differences may exist between them. Variances in key substances could potentially impact the functions of these vesicles. This is particularly notable for bacterial-derived vesicles, which necessitate a complex pre-treatment process before acquisition. This process can influence their PAMPs, potentially altering their immune function, and may also give rise to other metabolites. Consequently, the direct applicability of NVs as a metabolite of EVs requires verification, and this article is dedicated to exploring this aspect.

In this study, we first systemically studied the differences between PSB-derived OMVs and BNVs in morphology, size, major membrane components, and lipid composition. Subsequently, we delved into an investigation of their divergent effects concerning tumor suppression and wound healing based on their differences in key beneficial elements. Our results showed that in terms of morphology and size, there were no substantial disparities between PSB-derived OMVs and BNVs. However, BNVs contained a greater abundance of active ingredients and metabolomics. Notably, comparing with OMVs, BNVs had heightened concentrations of lysophosphatidylcholine (LPC), a phospholipid with hemolytic properties. LPC is the main component of oxidized low-density lipoprotein (oxLDL), which causes oxidative damage. Moreover, LPC exerts physiological activities, including the stimulation of vascular smooth muscle cell proliferation, instigation of extracellular matrix protein generation, and suppression of inflammatory mediators [21]. Furthermore, LPC can be metabolized by LPC acyltransferase (LPCAT) to generate phosphocholine (PC), which promotes cell proliferation and activates downstream signals for promoting angiogenesis and epithelialization [22]. Consequently, BNVs enriched with LPCs emerge as the optimal candidates for enhancing wound healing processes. In the wound healing model, our results indicated that while both OMVs and BNVs facilitated NIH 3T3 cell proliferation, migration, and activation of the EGFR/AKT/PI3K pathway, BNVs showcased superior efficacy in expediting wound closure. Shifting the focus to cancer therapy, we observed a contrary outcome: OMVs exhibited enhanced anti-tumor activity by polarizing macrophages toward the M1 phenotype and augmenting the release of inflammatory cytokines compared to BNVs. In essence, our investigation furnishes a promising methodology and criteria for discerning the suitability of nanovesicles in treating distinct diseases (Scheme 1).

2. Results

2.1. Characterizations and detection of active ingredient of OMVs and BNVs

The schematic diagram of the BNVs preparation process was shown in Fig. 1a. As a cell traversed a micropore, the cell membrane underwent extension due to adhesive tension, leading to the release of cell membrane fragments (lipid bilayer fragments) into the aqueous phase. The amphiphilic nature of these lipid bilayer fragments caused them to spontaneously transition into vesicles in the aqueous environment. Earlier studies suggested that lipid bilayer fragments exceeding 50 nm in length adopted a spherical vesicular shape, as this configuration minimized free energy [23,24]. Initially, the morphology and size characterization were conducted using TEM. OMVs and BNVs had the same morphology and size, they were spherical and saccular structure with a uniform size of about 100 nm (Fig. 1b and c). PSB, classified as Gram-negative bacteria within prokaryotic microorganisms, lacks typical nuclear structures and conventional organelles with membrane encapsulation, such as ribosomes. Notably, OMVs and BNVs primarily consist of lipid bilayers. Even if there are organelles with membrane structures, the extrusion process compresses them into fragments, subsequently transforming into vesicles due to their amphiphilic nature in the aqueous phase. In summary, the influence of organelles and nuclei on the performance characteristics of OMVs and BNVs can be considered negligible [2]. Subsequently, we used DLS to characterize their size. The size distribution of OMVs spans 170–300 nm, with a pronounced peak around 220 nm (Fig. S1a). Correspondingly, the distribution of BNVs ranges from 160 to 260 nm, with the most prominent concentration centered at approximately 200 nm. Furthermore, the size and concentration were detected by NTA. The results showed that the sizes of OMVs and BNVs were between 0 and 300 nm. OMVs were mainly distributed around 99 nm (Fig. 1e) while BNVs were mainly distributed around 125 nm (Fig. 1f). Additionally, it was determined that each batch of 5×10^9 CFU PSB has the capacity to yield 1.3×10^{10} BNVs, highlighting a noteworthy production efficiency. In addition, the materials obtained from different batches remained stable to a certain extent (Fig. S1).

PSB are abundant in chlorophyll, a crucial element for photosynthesis [4]. When formed, OMVs carry cytoplasmic components, including a small amount of chlorophyll [11]. We hypothesize that during the extrusion process of BNVs, the membrane and cell contents recombine, potentially resulting in a higher chlorophyll content. The schematic diagram of OMVs and BNVs is depicted in Fig. 1d. Notably, the levels of chlorophyll *a*, chlorophyll *b*, and total chlorophyll in BNVs were significantly higher than those in OMVs, as illustrated in Fig. 1j.

Upon treatment with lysozyme, the cell wall of PSB undergoes partial dissolution. As LPS is present on the cell wall of PSB, a lower LPS content signifies a higher dissolution of the cell wall, rendering subsequent operations more convenient. In the case of BNVs, there was no significant difference in LPS content between the 20 min treated group and the untreated group, as depicted in Fig. 1g. However, the LPS content on the

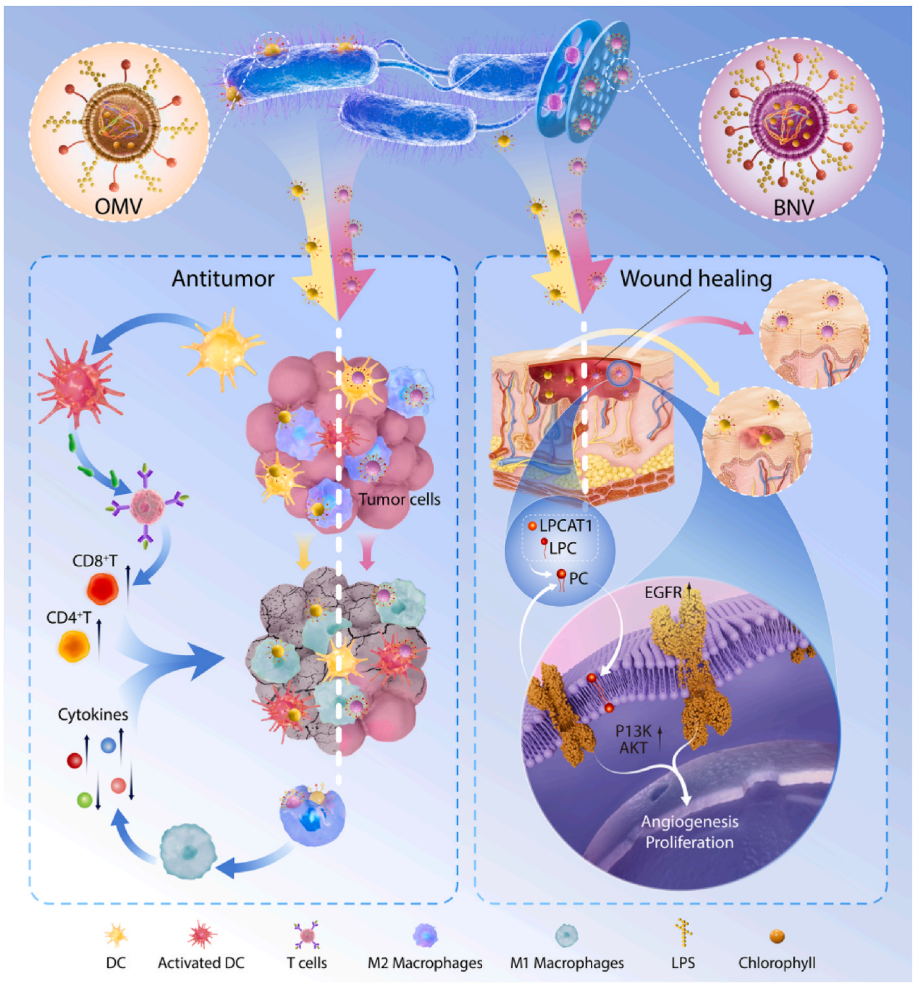

Scheme 1. Investigating the variations in composition and functionality between OMVs and BNVs derived from photosynthetic bacteria in terms of their anti-tumor effects and promotion of wound healing.

surface of BNVs exhibited a notable reduction after treatment durations of 30 min or more. Furthermore, at treatment durations of 30, 60, 90, and 120 min, no significant variations were observed in the LPS content adorning the BNVs surface. Consequently, the optimal preparation time of 30 min was adopted. Under identical conditions, the levels of LPS and PG in BNVs were significantly higher than those in OMVs, as indicated in Fig. 1h and i. This disparity suggested noticeable distinctions in their structural compositions, likely stemming from divergent production processes.

2.2. Metabolomics results

In this study, an extensive metabolomics analysis of OMVs and BNVs was undertaken. The differential metabolites between each group were examined using a combination of multi-dimensional and single-dimensional approaches. A volcanic map was employed to visually represent the P value, Variable Important in Projection (VIP), and Fold change value, facilitating the identification of differential metabolites. The findings displayed distinctive patterns: prominently up-regulated metabolites were depicted by the red origin, conspicuously down-regulated metabolites by the blue origin, and metabolites undergoing negligible alteration by the gray points (Fig. 2b). According to statistical analysis, 4967 metabolites were included in the analysis of OMVs and BNVs. Among them, 4503 metabolites exhibited no significant difference. In comparison with OMVs, 3740 metabolites were significantly up-regulated, and 1298 metabolites were significantly down-regulated in BNVs.

To visually highlight the variations in metabolite expressions among various samples, hierarchical clustering analysis was performed on selected metabolites exhibiting significant differences. The cluster heatmap of all differential metabolite results was presented (Fig. S2), where the horizontal axis corresponds to the sample names, and the vertical axis corresponds to the varying metabolites. The intensity of the red coloration in the figure directly corresponds to the abundance of expression of these differing metabolites; deeper shades of red indicate higher expression levels.

The lipids among the distinct metabolites mentioned earlier underwent further analysis, including the classification and quantity of lipid metabolites (Fig. 2a). In total, there were 9 kinds, with the largest number of fatty acids, followed by pentenol lipids, and then glycerophospholipids. The results of hierarchical clustering were presented in Fig. 2d. The pathway enrichment analysis of differential metabolites was helpful in understanding the mechanism of metabolic pathway changes in differential samples. We analyzed the metabolic pathway enrichment of lipids in differential metabolites based on KEGG database (accessible at https://www.kegg.jp/). Significant enrichment pathways were selected for sankey-bubble diagram (Fig. 2e). The leftword sankey diagram showed the metabolites corresponding to each pathway. In the rightward bubble chart, the ordinate represents the name of the metabolic pathway, while the abscissa represents the enrichment factor denoted by the Rich factor. The Rich factor is calculated as the ratio of significantly different metabolites to the total metabolites within the pathway.

The color gradient from green to red signifies a decrease in P-value.

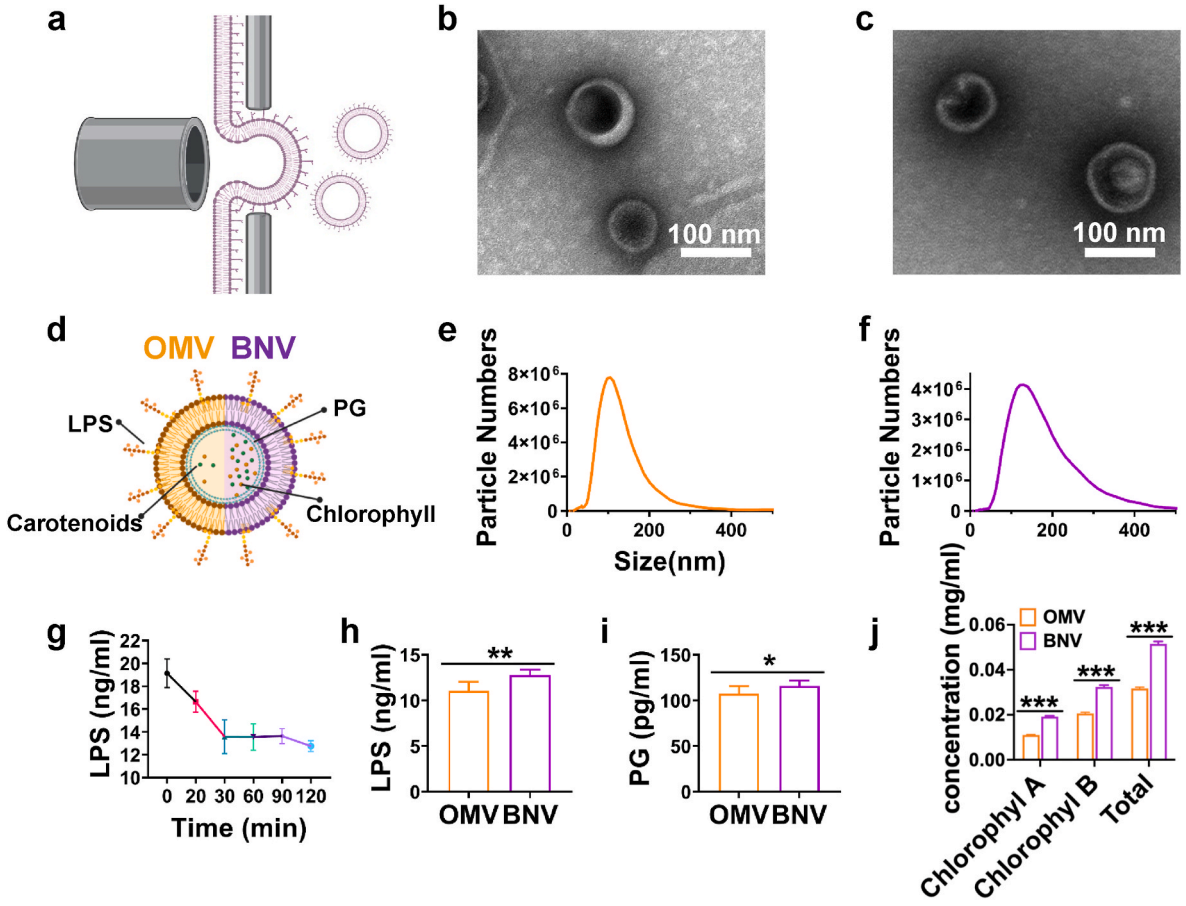

Fig. 1. Characterization of OMVs and BNVs. (a) Schematic diagram of the preparation of BNVs. (b) TEM images of OMVs. (c) TEM images of BNVs. (d) Schematic diagram of OMVs and BNVs. (e) NTA analysis of OMVs. (f) NTA analysis of BNVs. (g) Analysis of LPS content on BNVs surface treated with lysozyme for different time. Analysis of (h) LPS and (i) PG content on OMVs and BNVs. (j) Analysis of chlorophyll content in OMVs and BNVs. (*$p < 0.05$, **$p < 0.01$, and ***$p < 0.001$).

Larger points indicate a higher enrichment of metabolites, and the redder the color, the smaller the P-value. The size of the bubbles corresponds to the number of differential metabolites, with larger bubbles representing a greater number. Clearly, our analysis highlights the paramount significance of arachidonic acid metabolism as the foremost pathway, closely followed by glycerophospholipid metabolism.

Following this, we conducted a comprehensive enumeration of the lipid differential metabolites mentioned earlier. Notably, within this array of distinct metabolites, LPC (17:0) emerged as the most prevalent one, prominently associated with Sphingolipid metabolism. A comparative assessment revealed that the content of LPC (17:0) in BNVs was higher than that in OMVs (Fig. 2c). The analysis of metabolites in this pathway was shown (Fig. S3). The Arachidonic acid metabolism had the largest number of differential metabolites, and the contents of each metabolite in this pathway (Fig. S4). We hypothesize that the observed variations could stem from the distinct generation processes of OMVs and BNVs. OMVs result from the foaming of the bacterial outer membrane, whereas BNVs are produced through extrusion. In the extrusion process, both internal and external membrane components undergo disassembly and reassembly, though the precise mechanism requires further investigation.

The LPC molecule exhibits the remarkable ability to stimulate the proliferation of vascular smooth muscle cells through MAPK pathway, while simultaneously fostering the synthesis of extracellular matrix proteins via the AKT pathway [21]. Furthermore, it demonstrates the potential to undergo conversion into PC through the intricate process of LPCAT-mediated metabolism. This metabolic transformation not only exerts an influence on the physical architecture of the cellular membrane but has also been substantiated as a trigger for the activation of the EGFR signaling cascade [22]. Within this intricate signaling web, the EGFR assumes a pivotal role in the intricate process of wound healing. The elevation of EGFR ligands and subsequent activation of downstream pathways such as EGFR-MEK-ERK and EGFR-PI3K-AKT collectively act in concert to stimulate key aspects of wound healing, including angiogenesis, epithelialization, and the orchestration of extracellular matrix components. As a consequence, this orchestrated symphony of cellular events significantly expedites the overall healing of skin wounds [25–27].

In addition, it is important not to overlook the functional influence of other substances in vesicles, e.g. proteins. Previously, Wen et al. profiled the proteomics of natural EVs (nEVs) and cell-derived nanovesicles (CNVs). Although the protein composition of nEVs and CNVs is different, the similarity of membrane proteins was found to be 70.7%, and the molecular functions of proteins in nEVs and CNVs are similar to a high extent [19]. In another study, Wang and coworkers demonstrated that MSC-derived NVs share a higher similarity in organelle-specific markers with MSCs compared to MSC EVs, suggesting that the EVs and NVs proteins inherited from the parental cells may not be the most critical ingredients for their therapeutic functions [28,29]. This finding is consistent with previous observations that lipid metabolism plays an important role in disease progression, as lipids are the major component of cell-derived vesicles. Certain exosomal lipids have been identified as key components of therapeutic effects in cancer therapy and wound healing [30,31]. Inspired by these pioneering studies, in this study we focus on profiling the lipid components in BNVs and OMVs and emphasize their impact on wound healing and anti-tumor therapy.

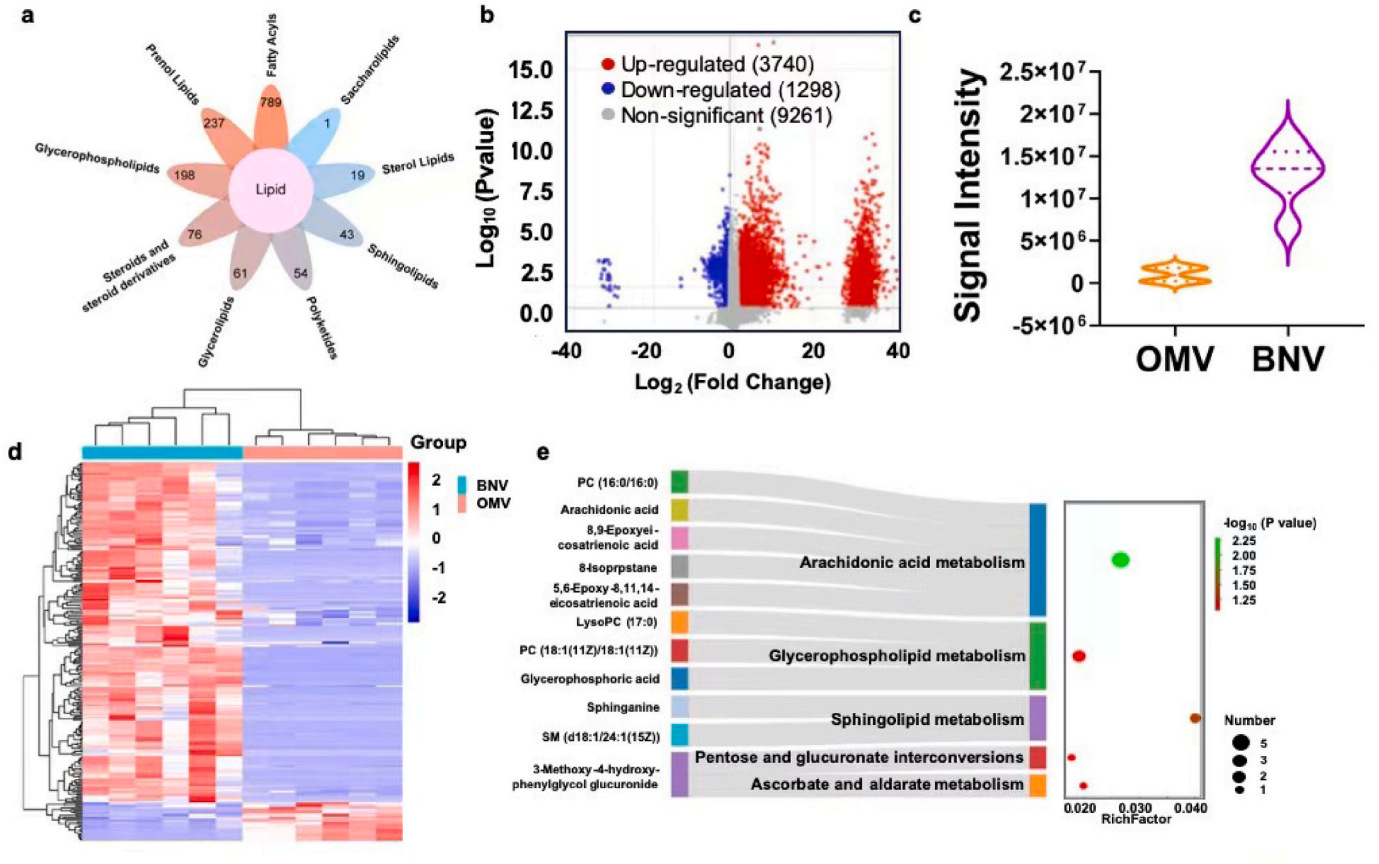

Fig. 2. Metabolomics analysis. (a) Classification and quantity of lipid metabolites. (b) Volcanic map of differential metabolites screened by VIP and P. (c) Analysis of the contents of LPC (17:0). (d) Cluster heatmap of lipid metabolites. (e) Sankey-bubble diagram of metabolic pathway.

2.3. OMVs and BNVs accelerate wound healing in vitro

In the context of wound treatment, ensuring safety is of paramount importance. Earlier studies have established that PSB is a non-toxic and non-pathogenic bacterium [1,32] Moreover, our research group has previously demonstrated that even live PSB bacteria can safely and effectively promote wound healing, thanks to the presence of various anti-inflammatory components such as carotenoids and CoQ10 [5]. These anti-inflammatory components serve to mitigate any side effects induced by PSB. In the context of this article, it's noteworthy that, compared to live bacteria, both OMVs and BNVs exhibit no replicability and higher safety profiles. Wound healing was completed through a trio of intertwined stages: the inflammatory stage, the proliferative stage, and the remodeling stage [33]. NIH 3T3 cells played a key role in these three stages. The proliferation and migration of NIH 3T3 cells were necessary for extracellular matrix synthesis and wound contraction [34,35]. We detected the proliferation and migration of NIH 3T3 cells after different treatments. Both BNVs and OMVs promoted the proliferation of NIH 3T3 cells, and the effect of BNV group was more significant (Fig. 3d). Similarly, both BNVs and OMVs promoted the migration of NIH-3T3 cells, with the former exhibiting a more pronounced impact (Fig. 3c and f).

Lipid metabolism was closely related to wound healing [36]. Theoretically, exogenous LPC carried by BNVs could undergo metabolism to generate PC under the catalysis of LPCAT1, consequently leading to changes in the membrane structure. This sequential process induces alterations in the membrane configuration, subsequently triggering the activation of the EGFR signaling cascade [22,37]. At the same time, EGFR signal would activate downstream PI3K/AKT pathway, promote cell proliferation and migration, and then accelerate wound healing process [38]. The schematic diagram of pathway activation was shown in Fig. 3a. We analyzed the activation of EGFR/PI3K/AKT pathway in NIH 3T3 cells by Western blot. After treatment with OMVs and BNVs, the expression of EGFR, PI3K and AKT all increased significantly, with the effect being more pronounced in the BNVs group (Fig. 3b–e and Fig. S5). It proved that LPC carried by BNVs promoted the proliferation and migration of NIH 3T3 cells through EGFR/PI3K/AKT pathway.

2.4. The effect of accelerating wound healing in vivo

The aforementioned study has substantiated that both OMVs and BNVs exert the capacity to enhance the proliferation and migration of NIH 3T3 cells through the activation of the EGFR/PI3K/AKT pathway. Furthermore, the outcomes uniformly demonstrate the superior advantages of BNVs over OMVs in the context of promoting wound healing. Subsequently, the effects of OMVs and BNVs in promoting wound healing was investigated *in vivo*. The experimental procedure was elucidated (Fig. 4a). During the initial days, the mice in all groups exhibited a reduction in body weight attributed to the excision of skin tissue. However, after the second day, the weight of all mice increased steadily, and there was no significant difference among the three groups (Fig. 4c). Thus, OMVs and BNVs exhibited commendable biocompatibility, evincing negligible adverse effects on the mice. The wound healing process and the closure rate of each group was recorded. The wound area of each group showed a decreasing trend during the monitoring process, and the decreasing trend of BNV group was significantly higher than other groups (Fig. 4b and d). H&E staining results showed that all three groups of mice had complete dermal tissue (Fig. 4e). However, there was still a large number of inflammatory cell infiltration in the control group, and there were almost no hair follicles

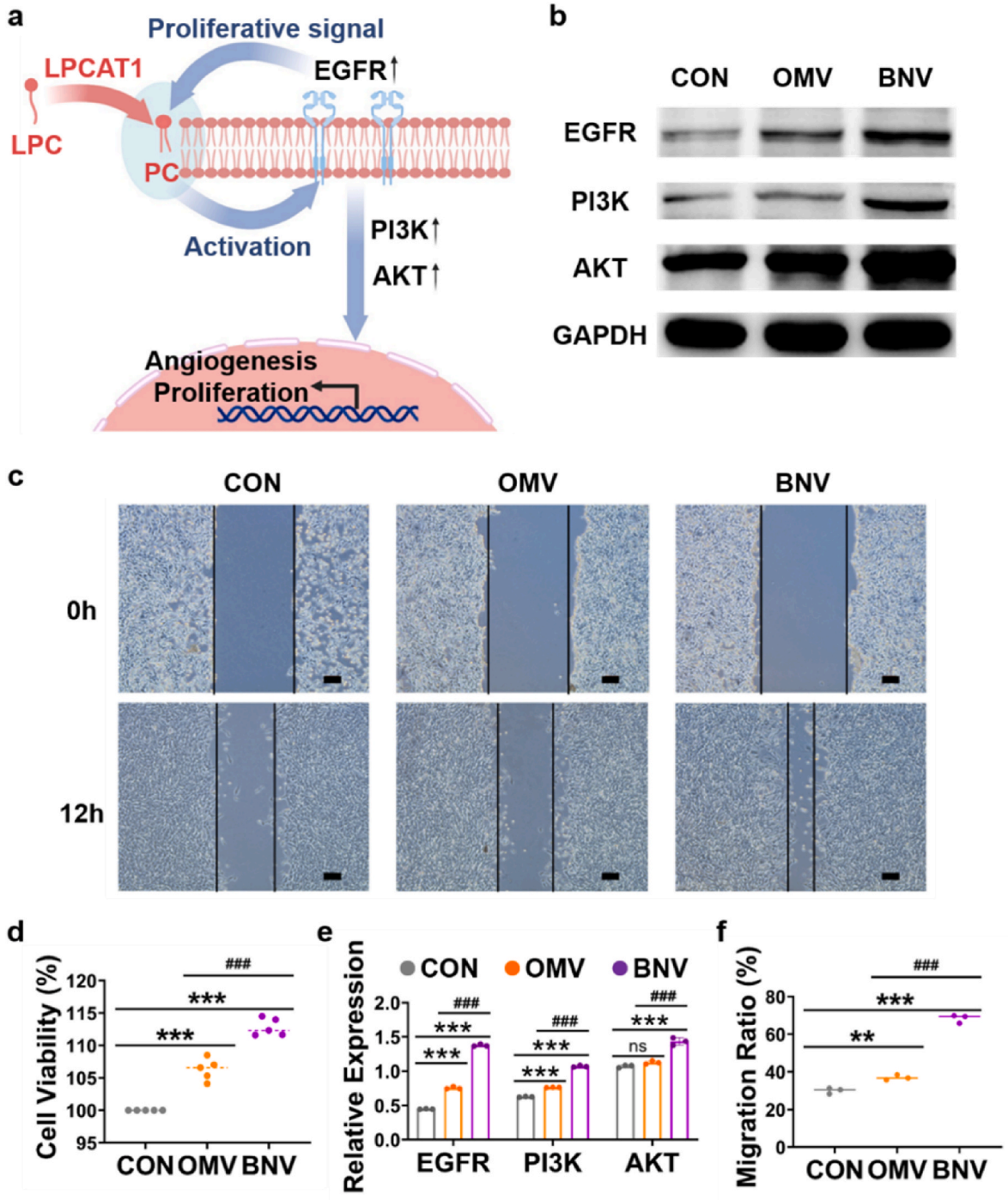

Fig. 3. Analysis of wound healing *in vitro*. (a) Schematic diagram of pathway activation. (b) Western blot analysis of EGFR/PI3K/AKT pathway. (c) Cell migration was measured by scratch test. (d) Proliferation ratio of NIH–3T3 cells. (e) Western blot quantitative analysis of EGFR/PI3K/AKT pathway. (f) Migration ratio of NIH–3T3 cells. (*, compared with con; #, BNV compared with OMV. $^{*}p < 0.05$, $^{**}p < 0.01$, and $^{***}p < 0.001$).

and glands. In the OMV group, there were a few inflammatory cells, including hair follicles and glands. Strikingly, the BNV group exhibited minimal inflammatory cell presence, alongside robust generation of hair follicles and glands, thus yielding the most efficacious healing effect. Masson staining results showed that compared with the control group, the collagen fibers and muscle fibers in OMV group were arranged more orderly. While the collagen fibers and muscle fibers in BNV group were arranged most orderly. It showed that BNVs had the best ability to promote wound healing.

TNF-α is a common inflammatory factor within wound sites. An overabundance of TNF-α can lead to the undesirable outcome of delayed wound healing [39]. CD31 is a transmembrane protein expressed in early angiogenesis. Increased expression of CD31 will accelerate angiogenesis and promote wound healing [40]. The inflammatory regulation and angiogenesis of OMVs and BNVs can be analyzed by IHC. As shown in Fig. 4f and i, it had the corresponding inflammatory factor (TNF-α) expression in all groups, but BNV group had the least positive cell count than other groups. When tissues collected, the wound in group OMV and BNV has almost healed, the inflammatory factors have definitely decreased. Thus, they have a lower expression of TNF-α. In

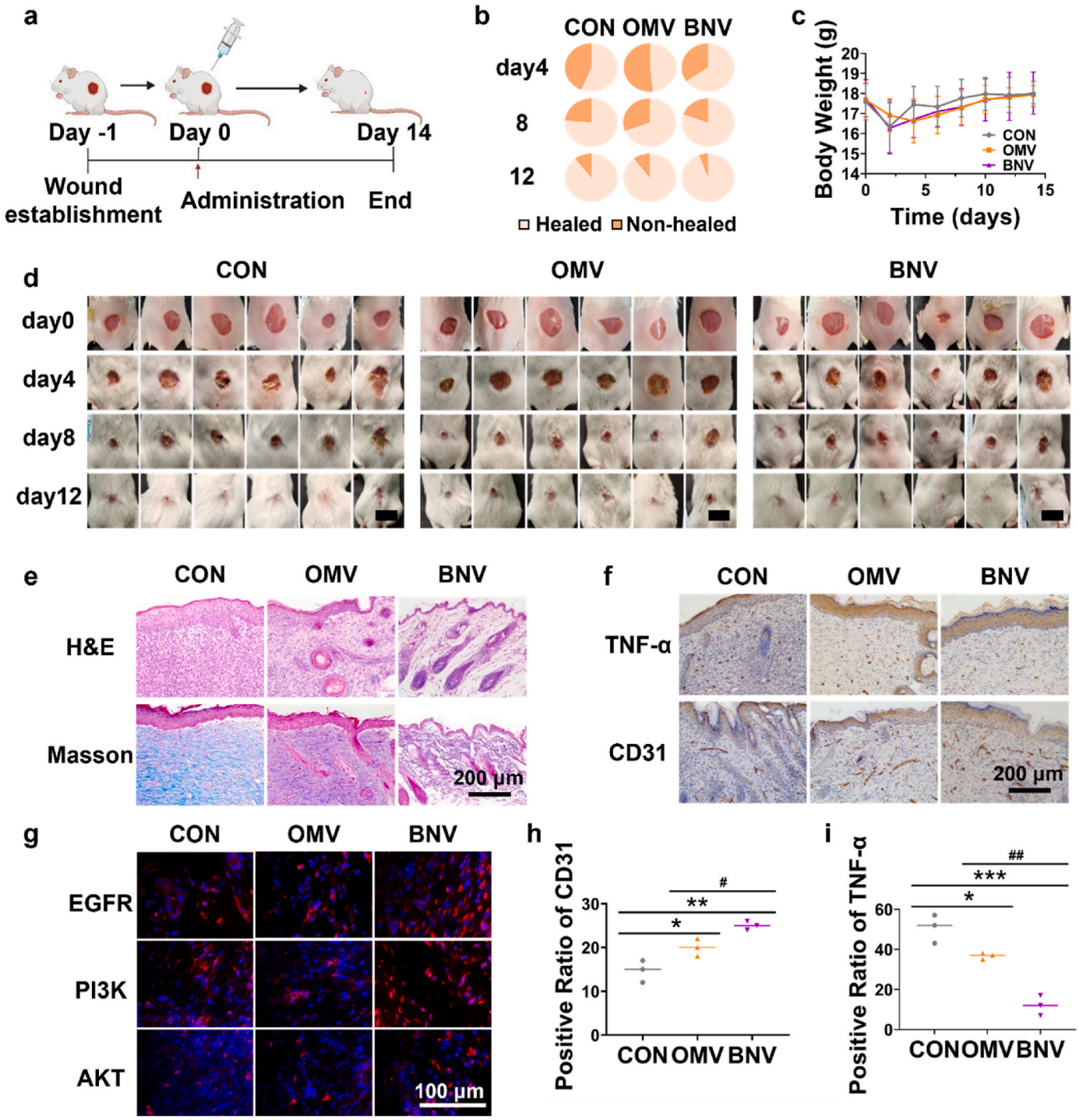

Fig. 4. The effect of accelerating wound healing *in vivo*. (a) Diagram of wound healing experiment. (b) The wound closure ratio. (c) Changes in body weight. (d) Images of wound healing process in mice. Scale bar is 1 cm. (e) H&E and Masson staining of skin tissue sections. (f) IHC of TNF-α and CD31. (g) IF analysis of EGFR/PI3K/AKT pathway. Positive ratio of (h) CD31 and (i) TNF-α. (*, compared with con; #, BNV compared with OMV. *$p < 0.05$, **$p < 0.01$, and ***$p < 0.001$).

addition, various anti-inflammatory components such as carotenoids and CoQ10 are contained in BNVs, which may offset the inflammatory response caused by LPS [5]. Therefore, the expression of TNF-α in group BNV is the lowest. As shown in Fig. 4f and h, the expression of CD31 in BNV group was the highest, which indicated that BNVs had better ability to facilitate angiogenesis. In summary, BNVs had a stronger ability to reduce inflammation and promote angiogenesis. In addition to the function of LPC, carotenoids from PSB and other components contained in BNVs could also play an antioxidant role, balance the redox pressure at the wound site and help regulate the inflammatory reaction [41].

As mentioned *in vitro*, BNVs promoted the proliferation and migration of NIH 3T3 cells through EGFR/AKT/PI3K pathway, which was also verified in this section *in vivo*. IF (Fig. 4g) and Western blot (Figs. S6 and S7) results showed that the expressions of EGFR, PI3K and AKT in OMV and BNV groups all increased significantly, and the changes in BNV group were more obvious. This proved that LPC carried by BNVs promoted wound healing in mice through EGFR/PI3K/AKT pathway.

In addition to promoting cell proliferation, LPC also plays a vital role

in nourishing nerves. It is involved in synthesizing the membrane required for neurogenesis and exerts a stimulating effect on neurocytes [42]. Notably, for neurodegenerative diseases like Alzheimer's, LPC may exhibit potential neuroprotective effects [43]. Furthermore, the rich carotenoids in BNVs offer anti-inflammatory and antioxidant effects, providing numerous health benefits, including the reduction of cancer and cardiovascular risks, and promoting heart protection [44].

2.5. The impact of OMVs and BNVs on immune microenvironment

OMVs carries LPS on its surface, which can be recognized and swallowed by macrophages via Toll like receptor (TLR) [45,46]. We observed the polarization effect of OMVs and BNVs on M2 macrophages and the activation effect on DC cells. Consequently, this interaction prompts a transformation of M2-type macrophages into M1-type macrophages (Fig. 5a). In order to detect the effects of OMVs and BNVs on the phenotype of macrophages, the expression of CD80, CD86, and CD206 was assessed. Among these, CD206 serves as a distinctive marker for M2-type macrophages, while CD80 and CD86 are hallmark proteins for M1-type macrophages [47]. Both OMVs and BNVs led to elevated expressions of CD80 and CD86 in macrophages, accompanied by a reduction in CD206 expression (Fig. 5c). Notably, the transformation induced by OMVs was the most pronounced. Therefore, *in vitro* results indicated that OMVs could polarize macrophages from M2 type to M1 type. Compared with BNVs, OMVs had more advantages in improving tumor immunosuppression microenvironment.

To further delve into the polarization of macrophages, we examined the cytokines secreted during their treatment. IL-6 and TNF-α are the primary secretions of M1 macrophages, exhibiting potential in anti-tumor capacities. Conversely, M2 macrophages primarily secrete IL-4 and IL-10, which tend to hinder the impact of tumor immunotherapy. We found an augmentation in the concentrations of IL-6 and TNF-α within the OMV and BNV groups, accompanied by a reduction in IL-4 and IL-10 levels (Fig. 5d). Notably, the OMV group displayed elevated levels of anti-tumor cytokines and diminished levels of immunosuppressive cytokines, in comparison to the BNV group.

In the intricate milieu of the tumor microenvironment, alongside macrophages, dendritic cells (DCs) stand as pivotal players in antigen presentation. DCs are typical full-time antigen presenting cells. However, DCs are generally immature within tumor, so their antigen presenting ability is poor. Yet, through strategic DCs activation, their capacity for antigen presentation can be potentiated, concomitantly heightening the expression of critical costimulatory molecules [48,49]. Notably, investigations have revealed that the maturation of DCs can be spurred by bacterial stimuli [50]. This insight fuels the presumption that OMVs hold the potential to rouse DCs into action, galvanizing their antigen-presenting function (Fig. 5b). Following the incubation of DCs with OMVs and BNVs separately, the levels of MHC I (Fig. S8), CD80 and MHC II (Fig. 5f) expression in DCs were assessed using FCM. Both OMVs and BNVs increased the expression of MHC I, MHC II and CD80, but the changes of OMVs were more obvious. Expanding the assessment to cytokine secretion, the secretion of cytokines was further detected by enzyme-linked immunosorbent assay (ELISA). OMVs and BNVs induced an increase in the expression of IL-6 and TNF-α in DCs, with the changes being more pronounced in the OMV group (Fig. 5e). In summary, both OMVs and BNVs effectively activated DCs, with OMVs demonstrating a particularly heightened efficacy.

2.6. The antitumor effect in vivo

To assess the *in vivo* anti-tumor effects of OMVs and BNVs, distinct treatments were administered to tumor-bearing mice in each group. The alterations in body weight and tumor volume of each group were meticulously recorded throughout the treatment period. The experimental process is illustrated in Fig. 6a. There were no significant differences observed in the fluctuations of body weight among all groups, as shown in Fig. 6b. Notably, OMVs demonstrated the ability to prolong the survival time of mice and enhance their overall survival rate, as depicted in Fig. 6c. More importantly, the control group exhibited a rapid increase in tumor volume, while the BNV group displayed a comparatively weaker tumor inhibitory effect, as evidenced by the data presented in Fig. 6d and e. Remarkably, the OMV group exhibited the strongest tumor inhibitory effect. The H&E results (Fig. 6f) showed that the tumor cells were significantly reduced, and the interstitial tissue was rich in OMV group. While, the number of tumor cells in BNV group was higher than that in OMV group, accompanied by focal necrotic and invasion of cells. In conclusion, the tumor inhibition effect of OMV was better than that of BNV group. The TUNEL staining results revealed a higher level of apoptosis in tumor cells in both the OMV group and BNV group compared to the control group. Notably, the apoptosis of tumor cells in the OMV group was the most significant (Figs. 6f and 7b). In summary, both OMVs and BNVs exhibited anti-tumor effects, with the effect of OMVs being more pronounced.

As depicted in Fig. 7a, it is highlighted that OMVs possess the capability to activate DCs and polarize macrophages. This activation results in the release of various cytokines, including TNF-α, IL-6, and IFN-γ, which exert a direct cytotoxic effect on tumor cells. Furthermore, OMVs play a crucial role in antigen presentation to T cells, thereby activating them. Within this context, $CD8^+$T cells release granzymes and perforin, inducing apoptosis in tumor cells. $CD4^+$T cells, while supporting $CD8^+$T cells, also secrete IFN-γ and TNF-α to directly contribute to the elimination of tumor cells. The aforementioned results showed that OMVs had the strongest anti-tumor effect in mice. *In vitro* experiments also proved that OMVs and BNVs could polarize macrophages into M1 phenotype. Therefore, OMVs and BNVs are expected to polarize M2-type macrophages in tumor sites into M1 type *in vivo*. The immunofluorescence (IF) results illustrated a significant increase in CD80 expression and a simultaneous decrease in CD206 expression within tumor tissues after treatments with both OMVs and BNVs (Fig. 7d), with the effect being more pronounced in the case of OMVs. FCM results demonstrated that treatments with OMVs and BNVs up-regulated the expression of CD80 and down-regulated the expression of CD206 (Fig. S9), with OMVs exhibiting a stronger effect. Consequently, both OMVs and BNVs were capable of polarizing macrophages within the tumor tissue into the M1 type, with the impact being more pronounced in the OMV group. This polarization is beneficial for enhancing the immunosuppressive nature of the TME and improving the efficacy of immunotherapy. The ELISA analysis results indicated that both OMVs and BNVs up-regulated IL-6 and TNF-α, while down-regulating IL-4 and IL-10 (Fig. 7c). This further confirmed the polarization of macrophages into the M1 phenotype. In summary, all the results consistently point to a more favorable role of OMVs in tumor treatment.

The main organs (comprising heart, liver, spleen, lung and kidney) of each experimental group were analyzed by H&E staining. The main organs of mice in each group had no obvious damage, indicating that OMVs and BNVs had no obvious toxic and side effects (Fig. S10). Relevant pharmacokinetic data are presented in Fig. S11. The results showed that both OMVs and BNVs would be gradually cleared from blood within 24 h. Simultaneously, the material exhibited favorable blood compatibility, as illustrated in Fig. S12. Distribution experiments in mice showed that both OMVs and BNVs had certain tumor accumulation capacity (Fig. S13).

The aforementioned experimental results have convincingly demonstrated that OMVs effectively inhibited the growth of tumors and improved the immunosuppressive in tumor areas. In order to test whether it can further cause immune response, the infiltration of T cells in tumor tissues was meticulously assessed by IF (Fig. 7d, Fig. S14) and FCM (Fig. S9). The results showed that OMVs and BNVs could effectively enhance the infiltration of $CD3^+CD4^+$ T cells and $CD3^+CD8^+$ T cells in tumor tissues, and the impact of OMVs was more pronounced compared to that of BNVs. These results strongly suggest that both OMVs and BNVs play a crucial role in promoting T cell activation within the TME. This

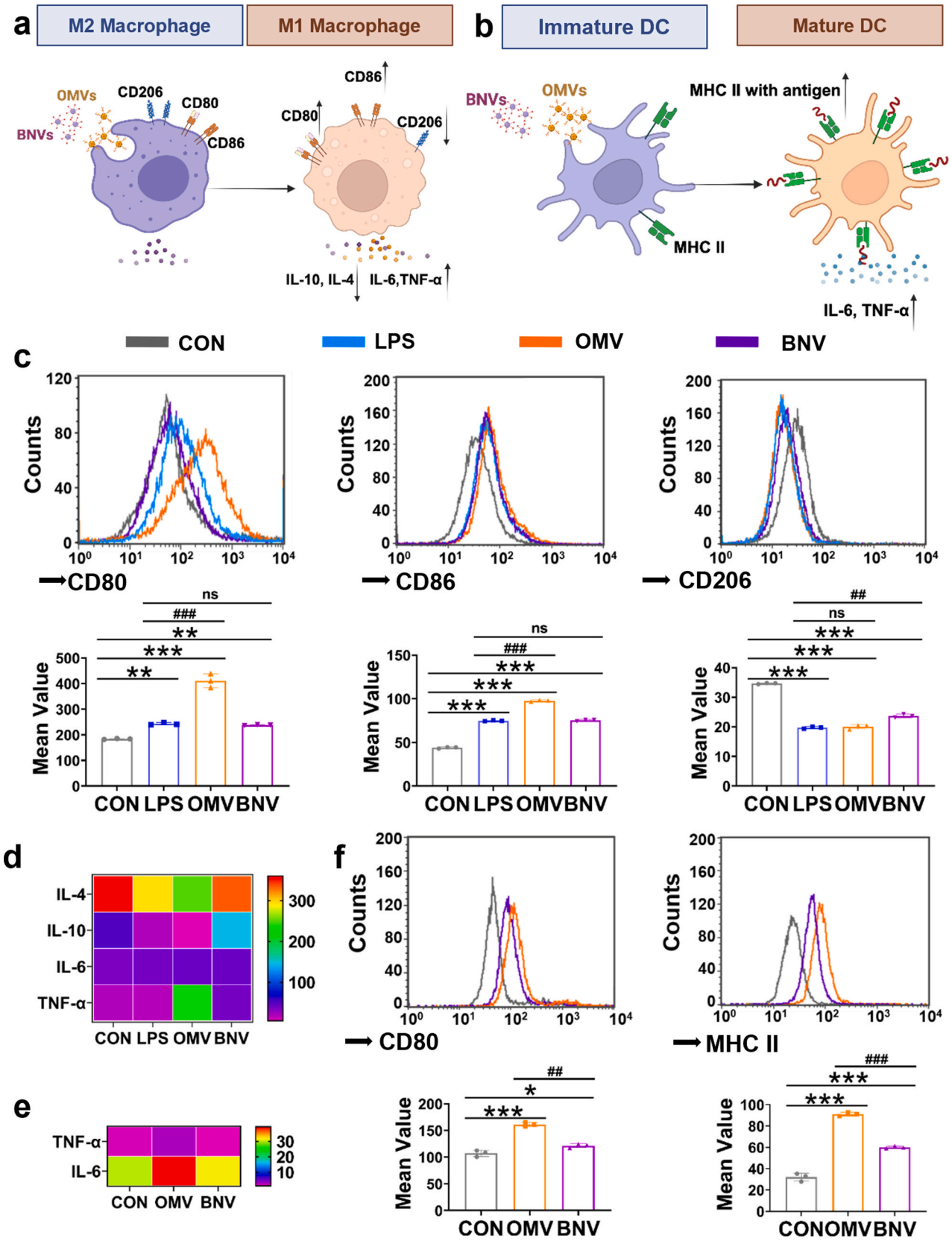

Fig. 5. Activation of macrophages and DCs. Schematic diagram of (a) macrophages polarization and (b) DCs activation. (c) FCM analysis of CD80, CD86 and CD206 in macrophages. (d) ELISA of IL-6, TNF-α, IL-4 and IL-10 in macrophages. (e) ELISA of IL-6 and TNF-α in DCs. (f) FCM analysis of CD80 and MHC II in DCs. (*, compared with con; #, BNV compared with OMV; ns, no significant difference. *$p < 0.05$, **$p < 0.01$, and ***$p < 0.001$).

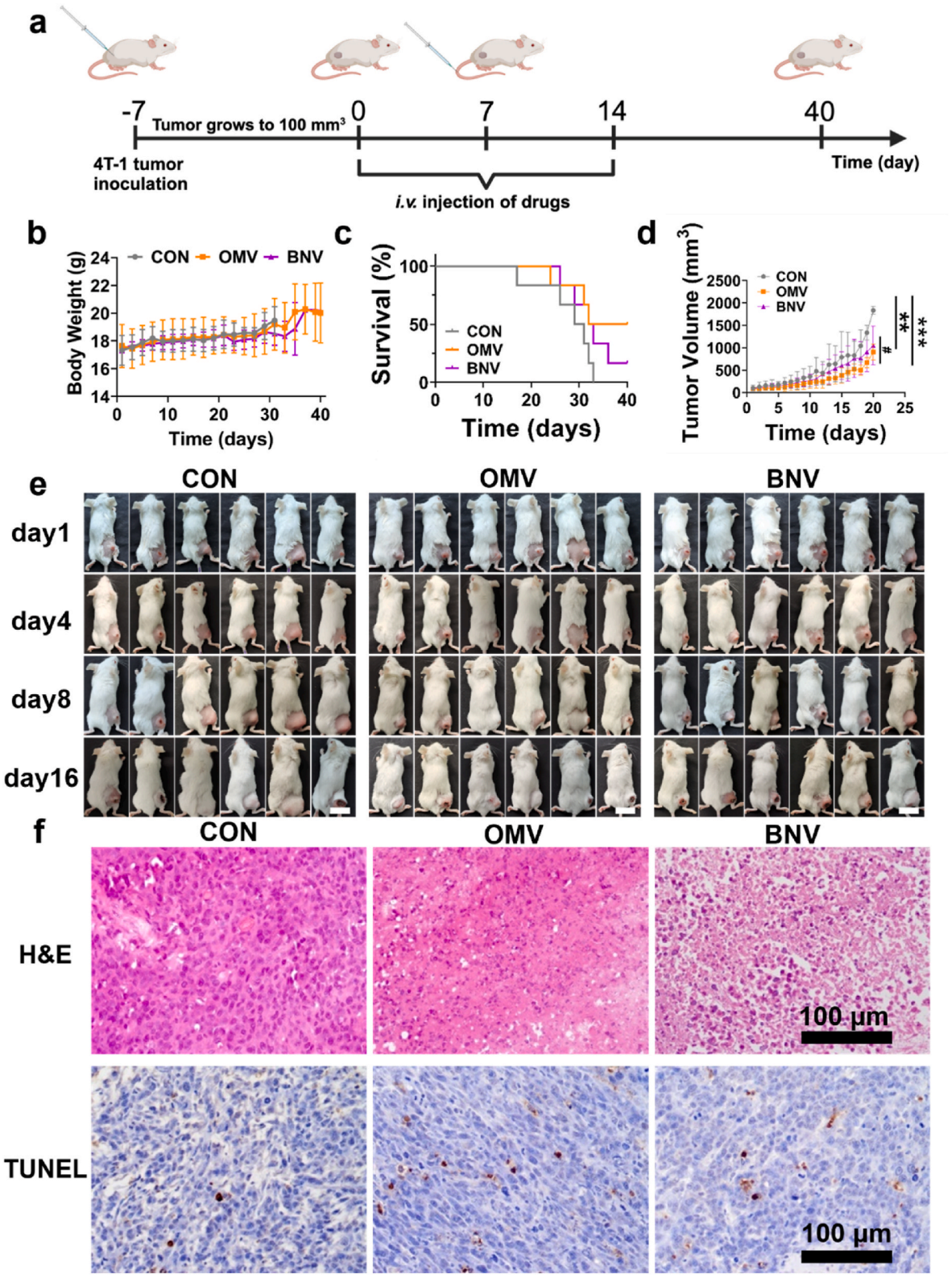

Fig. 6. The antitumor effect *in vivo*. (a) A diagram of tumor suppressing experiment. (b) Changes of body weight. (c) Survival rate of mice. (d) Tumor volume changes of mice during the treatment period. (e) Images of tumor-bearing mice. Scale bar is 2 cm. (f) H&E and TUNEL analysis of tumor tissues. (*, compared with con; #, BNV compared with OMV. $^{*}p < 0.05$, $^{**}p < 0.01$, and $^{***}p < 0.001$).

effect can be attributed to their synergistic impact on alleviating immunosuppression and enhancing macrophage-mediated antigen presentation. Notably, OMVs exhibited superior potency compared to BNVs, underscoring their enhanced therapeutic potential. Moreover, OMVs and BNVs, characterized by high immunogenicity, hold promise as vaccine antigen candidates in research and development aimed at preventing infectious diseases [51,52].

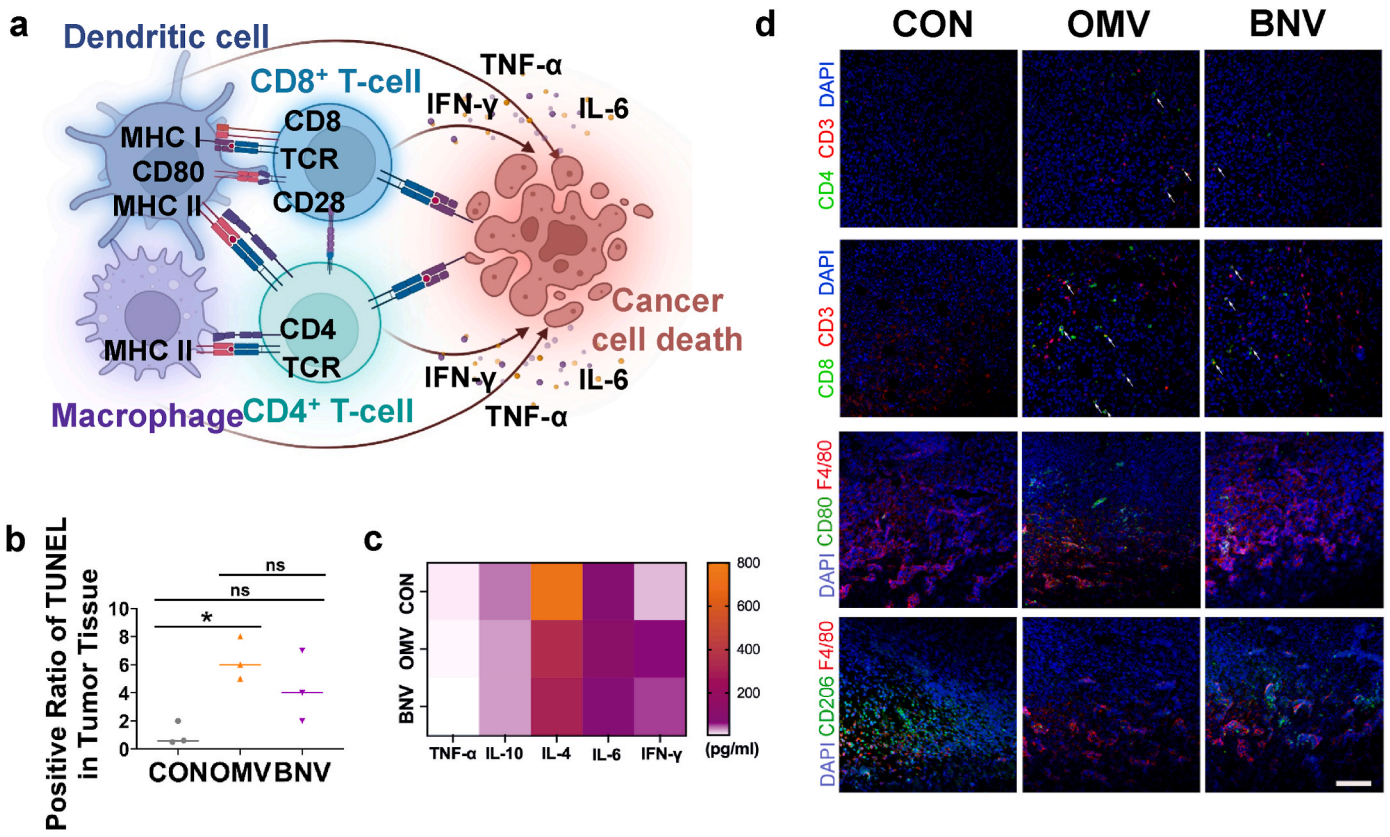

Fig. 7. Activation of macrophages, T cells and DCs *in vivo*. (a) A diagram of infiltration of immune cells in tumor tissue. (b) Positive ratio of TUNEL in tumor tissue. (c) ELISA analysis of the serum cytokine content in different treatment groups. (d) IF analysis of CD4, CD8, CD80 and CD206 in tumor tissues, scale bar is 50 μm. (*, compared with con; ns, no significant difference. $^{*}p < 0.05$, $^{**}p < 0.01$, and $^{***}p < 0.001$).

3. Conclusions

In essence, leveraging their photothermal properties and antioxidant abilities, PSB hold promise as a potential candidate for drug development or as a drug delivery system to address tumor and wound infections. However, practical application has been hindered by challenges such as substantial size and limited biosecurity. To address these issues, the emergence of OMVs and BNVs has provided partial solutions. Nonetheless, a comprehensive understanding of the distinctions between OMVs and BNVs remains elusive. Our study systematically explores the disparities between OMVs and BNVs originating from PSB.

Our findings reveal minimal differences in the morphology and size of OMVs and BNVs. However, significant variations exist in their active component contents and lipid compositions. Furthermore, *in vivo* experiments demonstrate that both vesicle types effectively inhibit tumor growth and enhance wound healing. Yet, OMVs excel in promoting macrophage polarization and immunopotentiation, resulting in a more pronounced anti-tumor effect. On the other hand, BNVs exhibit superior proficiency in promoting wound healing through the AKT pathway.

In summary, this study pioneers the elucidation of compositional and functional contrasts between OMVs and BNVs derived from PSB. It provides foundational insights for establishing production guidelines and biomedical applications of OMVs and BNVs technologies.

4. Materials and methods

4.1. Preparation of OMVs and BNVs

The schematic diagram of the preparation of BNVs is illustrated in Fig. 1a. The process involves incubating PSB in a liquid medium at 30 °C under light conditions. The bacterial supernatant is then subjected to filtration and centrifugation at 100,000 g for 2 h to obtain outer membrane vesicles OMVs.

For BNV preparation, PSB undergoes lysozyme treatment, followed by sequential extrusion through polycarbonate membrane filters with pore sizes of 1 μm, 600 nm, and 400 nm, each performed twice. The resulting solution is then ultrafiltered and can be stored at 4 °C or −80 °C.

4.2. Detection of active ingredient in OMVs and BNVs

The quantity of LPS, PG and chlorophyll of OMVs and BNVs were detected with kits according to the manufacturer's instructions.

4.3. The metabolomics analysis of OMVs and BNVs

The OMVs and BNVs samples underwent C18 column filtration, and 3 mL of methanol eluent was collected. Subsequently, 20 μL of the internal standard (L-2-chlorophenylalanine, 0.06 mg/mL, prepared in methanol) was added to the samples. In a glass vial, 1 mL of pre-cooled methanol-water (in a 4:1 of V:V ratio) was introduced twice. Following this, 200 μL of chloroform was added, and the solution was blown away with a pipette. Ultrasonic crushing was carried out in an ice bath.

The entire liquid was then transferred to a centrifuge tube, and ultrasonic treatment in an ice water bath was performed for 20 min. Subsequently, the samples were centrifuged at 4 °C (13,000 rpm) for 10 min. The supernatants from each tube were collected using crystal syringes, filtered through 0.22 μm microfilters, and transferred to LC vials. The vials were stored at −80 °C until LC-MS analysis. Quality control (QC) samples were generated by combining portions of all individual samples to create a pooled sample.

The metabolic profiling analysis was performed using an ACQUITY UPLC I-Class system (Waters Corporation, Milford) coupled with a Q-Exactive Plus quadrupole-Orbitrap mass spectrometer. The mass spectrometer was equipped with a heated electrospray ionization (ESI) source from Thermo Fisher Scientific (Waltham, MA). The investigation covered both ESI positive and ESI negative ion modes. The ACQUITY UPLC HSS T3 column was consistently utilized for both modes.

4.4. Proliferation and migration of NIH 3T3

NIH-3T3 cell culture was employed to assess the cell proliferation rate through the CCK-8 assay. After 24 h of culturing NIH-3T3 cells, a straight line was gently scraped across the fused cell layer using the tip of a sterilized straw. Following the addition of the material (10^8 particles/mL), the cells were cultured for an additional 24 h. The migration dynamics of NIH-3T3 cells were carefully examined using an optical microscope, specifically the Leica DMi8 model. The extent of migration was quantified by comparing the initial and post-experiment scratch widths. The PBS group served as the control group.

4.5. Western blot analysis

OMVs, BNVs and PBS were added into the culture system of NIH-3T3. After incubating, the cells were washed, lysed by lysate containing protease inhibitor. After centrifugation, the supernatant was collected and stored at −80 °C. After protein quantification, the content of EGFR, PI3K and AKT were analyzed by Western blot.

4.6. Wound healing experiment in vivo

The animal experimentation procedures strictly adhered to the guidelines established by the Experimental Animal Ethics Committee of Hebei University (Approval No. 2020XS074). Female BALB/c mice, 5 weeks old, were divided into 3 groups with 6 mice in each group. A circular full-thickness skin wound, measuring 1 cm in diameter, was created on the dorsal region of each mouse. After 24 h, 200 μL samples (10^9 particles/mL) were subcutaneously injected around the wound. Wounds treated with a saline solution served as the negative control. The physical condition of the mice, including their weight and the progress of wound closure, was systematically assessed and recorded at designated intervals. The calculation formula is as follows:

$$\text{Wound closure } (\%) = (W-Wn)/W \times 100\%$$

(W: Day 0 wound area; Wn: Day n wound area)

To assess both epidermal regeneration and inflammation within the wound area, skin samples were harvested and fixed in a 10% formaldehyde solution. Subsequently, these samples underwent processing to generate paraffin sections suitable for various analyses, including immunohistochemistry (IHC), H&E staining, and Masson staining. The activation of the EGFR/PI3K/AKT pathway was detected through Western blot and immunofluorescence (IF).

4.7. Macrophage polarization in vitro

Due to the substantial content of LPS in both OMVs and BNVs, their polarization effect on macrophages was observed. RAW 264.7 cells were seeded into a well plate. Following cell adhesion, OMVs (10^8 particles/mL), BNVs (10^8 particles/mL), and PBS were added. The cells were then treated with PE anti-mouse CD80, PE anti-mouse CD86, and FITC anti-mouse CD206 for labeling. FCM was employed to analyze the resulting polarization effect. To assess macrophage-related cytokines such as IL-10, IL-4, TNF-α, and IL-6, ELISA kits were utilized following the manufacturer's protocols.

4.8. Dendritic cells activation in vitro

Dendritic cells (DC 2.4) were obtained from Procell company. DCs were placed into a well plate, and subsequently, OMVs (10^8 particles/mL), BNVs (10^8 particles/mL), and PBS were added. The cells were then labeled with Rabbit Anti-MHC Class II/HLA DMB/FITC and PE anti-mouse CD80. The activation was analyzed by FCM. Additionally, IL-10, IL-6, TNF-α, and IL-4 were detected using ELISA kits. Placed DCs into well plate, then added OMVs, BNVs and PBS. The cells were then labeled with Rabbit Anti-MHC Class II/HLA DMB/FITC and PE anti-mouse CD80. The activation was analyzed by FCM. IL-10, IL-6, TNF-α, and IL-4 were detected by ELISA kits.

4.9. Antitumor experiments in vivo

Healthy BALB/c mice (5 weeks old, 20 ± 2 g, female) were selected for the study. After successfully modeling the 4T1 breast cancer tumor model, the mice were divided into three groups (CON, OMV, and BNV; n = 6). Over three cycles, each spanning 7 days, the mice underwent interventions. These interventions involved the administration of PBS (200 μL), OMVs (200 μL, 10^9 particles/mL), and BNVs (200 μL, 10^9 particles/mL) via the tail vein. Throughout this therapeutic period, the mice were attentively monitored for their survival, and meticulous measurements of tumor volumes and body weights were recorded. H&E staining, IF, and FCM were employed to detect tumor inhibition and immune cell infiltration in mice. Additionally, the levels of crucial cytokines (IL-6, IL-4, IL-10, and TNF-α) in the serum were assayed using ELISA.

Data availability

Data will be made available on request.

Ethics approval and consent to participate

All the animal experiments were approved by the Ethics Committee of Hebei University (Approval number: IACUC- 2020–016). All the authors were in compliance with all relevant ethical regulations.

CRediT authorship contribution statement

Tingshan Xiao: Writing – original draft, Methodology, Investigation, Formal analysis, Data curation. **Yichuan Ma:** Writing – original draft, Investigation, Formal analysis. **Ziyang Zhang:** Writing – original draft, Investigation. **Yixin Zhang:** Writing – review & editing, Investigation. **Yu Zhao:** Writing – review & editing, Investigation. **Xiaohan Zhou:** Methodology, Investigation. **Xueyi Wang:** Methodology, Investigation. **Kun Ge:** Methodology, Investigation, Data curation. **Junshu Guo:** Methodology, Investigation. **Jinchao Zhang:** Writing – review & editing, Validation, Resources, Funding acquisition. **Zhenhua Li:** Writing – review & editing, Funding acquisition, Conceptualization. **Huifang Liu:** Writing – review & editing, Writing – original draft, Validation, Project administration, Funding acquisition, Formal analysis, Conceptualization.

Declaration of competing interest

The authors declare that they have no known competing financial interests or personal relationships that could have appeared to influence the work reported in this paper.

Acknowledgements

This work was supported by the National Natural Science Foundation of China (32322045, 32271420, 31971304, and 21977024). The Beijing-Tianjin-Hebei Basic Research Cooperation Project

(19JCZDJC64100). Cross-Disciplinary Project of Hebei University (DXK201916). One Hundred Talent Project of Hebei Province (E2018100002). National High-End Foreign Expert Recruitment Plan (G2022003007L). Science Fund for Creative Research Groups of Nature Science Foundation of Hebei Province (B2021201038). Natural Science Foundation of Hebei Province (B2023201108). Hebei Province Higher Education Science and Technology Research Project (JZX2023001).

We are grateful to Medical Comprehensive Experimental Center of Hebei University for the animal experiment.

Appendix A. Supplementary data

Supplementary data to this article can be found online at https://doi.org/10.1016/j.bioactmat.2024.02.025.

References

[1] H.F. Lu, G.M. Zhang, Z.Q. Zheng, F. Meng, T.S. Du, S.C. He, Bio-conversion of photosynthetic bacteria from non-toxic wastewater to realize wastewater treatment and bioresource recovery: a review, Bioresource Technol. 278 (2019) 383–399.
[2] N. Pfennig, Photosynthetic bacteria, Annu. Rev. Microbiol. 21 (1967) 285–324.
[3] P.L. Zheng, M. Fan, H.F. Liu, Y.H. Zhang, X.Y. Dai, H. Li, X.H. Zhou, S.Q. Hu, X. J. Yang, Y. Jin, N. Yu, S.T. Guo, J.C. Zhang, X.J. Liang, K. Cheng, Z.H. Li, Self-propelled and near-infrared-phototaxic photosynthetic bacteria as photothermal agents for hypoxia-targeted cancer therapy, ACS Nano 15 (1) (2021) 1100–1110.
[4] E.M. Zhao, T.S. Xiao, Y.L. Tan, X.H. Zhou, Y.Q. Li, X.Y. Wang, K.H. Zhang, C.W. Ou, J.C. Zhang, Z.H. Li, H.F. Liu, Separable microneedles with photosynthesis-driven oxygen manufactory for diabetic wound healing, ACS Appl. Mater. Interfaces 15 (6) (2023) 7725–7734.
[5] E.M. Zhao, H.F. Liu, Y.R. Jia, T.S. Xiao, J.X. Li, G.Q. Zhou, J.N. Wang, X.H. Zhou, X. J. Liang, J.C. Zhang, Z.H. Li, Engineering a photosynthetic bacteria-incorporated hydrogel for infected wound healing, Acta Biomater. 140 (1) (2022) 302–313.
[6] D.D. Han, X. Zhang, Y.C. Ma, X.J. Yang, Z.H. Li, The development of live microorganism-based oxygen shuttles for enhanced hypoxic tumor therapy, Mater. Today Bio. 18 (2023) 100517.
[7] H.Y. Yan, M. Fan, H.F. Liu, T.S. Xiao, D.D. Han, R.J. Che, W. Zhang, X.H. Zhou, J. N. Wang, C. Zhang, X.J. Yang, J.C. Zhang, Z.H. Li, Microbial hydrogen "manufactory" for enhanced gas therapy and self-activated immunotherapy via reduced immune escape, J. Nanobiotechnol. 20 (2022) 280.
[8] Y.H. Zhang, H.F. Liu, X.Y. Dai, H. Li, X.H. Zhou, S.Z. Chen, J.C. Zhang, X.J. Liang, Z.H. Li, Cyanobacteria-based near-infrared light-excited self-supplying oxygen system for enhanced photodynamic therapy of hypoxic tumors, Nano Res. 14 (2020) 667–673.
[9] Q. Chen, H. Bai, Z.W.T. Wu, G.J. Huang, Y. Li, M. Wu, G.P. Tang, Y. Ping, Bioengineering bacterial vesicle-coated polymeric nanomedicine for enhanced cancer immunotherapy and metastasis prevention, Nano Lett. 20 (1) (2020) 11–21.
[10] G.X. Liu, L.N. Yang, G. Chen, F.H. Xu, F.H. Yang, H.H. Yu, L.N. Li, X.L. Dong, J. J. Han, C. Cao, J.Y. Qi, J.Z. Su, X.H. Xu, X.X. Li, B. Li, A review on drug delivery system for tumor therapy, Front. Pharmacol. 12 (2021) 735446.
[11] C. Schwechheimer, M.J. Kuehn, Outer-membrane vesicles from gram-negative bacteria: biogenesis and functions, Nat. Rev. Microbiol. 13 (2015) 605–619.
[12] M. Kaparakis-Liaskos, R.L. Ferrero, Immune modulation by bacterial outer membrane vesicles, Nat. Rev. Immunol. 15 (2015) 375–387.
[13] M. Spanos, P. Gokulnath, E. Chatterjee, G. Li, D. Varrias, S. Das, Expanding the horizon of EV-RNAs: LncRNAs in EVs as biomarkers for disease pathways, Extracell. Vesicle 2 (2023) 100025.
[14] K.D. Popowski, B. López de Juan Abad, A. George, D. Silkstone, E. Belcher, J. Chung, A. Ghodsi, H. Lutz, J. Davenport, M. Flanagan, J. Piedrahita, P.C. Dinh, K. Cheng, Inhalable exosomes outperform liposomes as mRNA and protein drug carriers to the lung, Extracell. Vesicle 1 (2022) 100002.
[15] W.L. Huang, L.X. Meng, Y. Chen, Z.Q. Dong, Q. Peng, Bacterial outer membrane vesicles as potential biological nanomaterials for antibacterial therapy, Acta Biomater. 140 (2022) 102–115.
[16] Z. Chen, Z. Qiao, C.R. Wirth, H.R. Park, Q. Lu, Arrestin domain-containing protein 1-mediated microvesicles (ARMMs) protect against cadmium-induced neurotoxicity, Extracell. Vesicle 2 (2023) 100027.
[17] A. Haltom, W. Hassen, J. Hensel, J. Kim, H. Sugimoto, B. Li, K. McAndrews, M. Conner, M. Kirtley, X. Luo, B. Xie, O. Volpert, S. Olalekan, N. Maltsev, A. Basu, V. LeBleu, R. Kalluri, Engineered exosomes targeting MYC reverse the proneural-mesenchymal transition and extend survival of glioblastoma, Extracell. Vesicle 1 (2022) 100014.
[18] S.C. Jang, O.Y. Kim, C.M. Yoon, D.S. Choi, T.Y. Roh, J. Park, J. Nilsson, J. Lotvall, Y.K. Kim, Y.S. Gho, Bioinspired exosome-mimetic nanovesicles for targeted delivery of chemotherapeutics to malignant tumors, ACS Nano 7 (2013) 7698–7710.
[19] Y. Wen, Q. Fu, A. Soliwoda, S. Zhang, M. Zheng, W. Mao, Y. Wan, Cell-derived nanovesicles prepared by membrane extrusion are good substitutes for natural extracellular vesicles, Extracell. Vesicle 1 (2022) 100004.
[20] O.Y. Kim, N.T. Dinh, H.T. Park, S.J. Choi, K. Hong, Y.S. Gho, Bacterial protoplast-derived nanovesicles for tumor targeted delivery of chemotherapeutics, Biomaterials 113 (2017) 68–79.
[21] P.P. Liu, W. Zhu, C. Chen, B. Yan, L. Zhu, X. Chen, C. Peng, The mechanisms of lysophosphatidylcholine in the development of diseases, Life Sci. 247 (2020) 117443.
[22] J. Bi, T.A. Ichu, C. Zanca, H. Yang, W. Zhang, Y. Gu, P.S. Mischel, Oncogene amplification in growth factor signaling pathways renders cancers dependent on membrane lipid remodeling, Cell Metab. 30 (3) (2019) 525–538.
[23] W. Jo, D. Jeong, J. Kim, J. Park, Self-renewal of bone marrow stem cells by nanovesicles engineered from embryonic stem cells, Adv. Healthc. Mater. 5 (24) (2016) 3148–3156.
[24] J. Yoon, W. Jo, D. Jeong, J. Kim, H. Jeong, J. Park, Generation of nanovesicles with sliced cellular membrane fragments for exogenous material delivery, Biomaterials 59 (2015) 12–20.
[25] A. Uchiyama, S. Nayak, S. Nayak, M.A. Cross, A. Overmiller, D. Grassini, M. Morasso, SOX2 Epidermal overexpression promotes cutaneous wound healing via activation of EGFR/MEK/ERK signaling mediated by EGFR ligands, J. Invest. Dermatol. 139 (8) (2019) S161.
[26] K. Xu, F.S. Yu, Impaired epithelial wound healing and EGFR signaling pathways in the corneas of diabetic rats, Invest. Ophth. Vis. Sci. 52 (6) (2011) 3301–3308.
[27] Q.W. Liu, J.C. Zhang, X.Y. Han, J. Chen, Y.T. Zhai, Y. Lin, H.K. Ma, F. Feng, X.J. He, P. Li, Huiyang Shengji decoction promotes wound healing in diabetic mice by activating the EGFR/PI3K/ATK pathway, Chin. Med. 16 (2021) 111.
[28] X. Wang, S. Hu, D. Zhu, J. Li, K. Cheng, G. Liu, Comparison of extruded cell nanovesicles and exosomes in their molecular cargos and regenerative potentials, Nano Res. 16 (5) (2023) 7248–7259.
[29] X. Wang, S. Hu, J. Li, D. Zhu, Z. Wang, J. Cores, K. Cheng, G. Liu, K. Huang, Extruded mesenchymal stem cell nanovesicles are equally potent to natural extracellular vesicles in cardiac repair, ACS Appl. Mater. Interfaces 13 (47) (2021) 55767–55779.
[30] B.F. Hettich, M. Ben-Yehuda Greenwald, S. Werner, J.C. Leroux, Exosomes for wound healing: purification optimization and identification of bioactive components, Adv. Sci. 7 (23) (2020) 2002596.
[31] L. Ye, Y. Li, S. Zhang, J. Wang, B. Lei, Exosomes-regulated lipid metabolism in tumorigenesis and cancer progression, Cytokine Growth F. R. (2023) 27–39.
[32] X. He, W. Guo, Y. Tang, J. Xiong, Y. Li, R. Huang, W. Miao, Chloroplast-boosted photodynamic therapy for effective drug-resistant bacteria killing and biofilm ablation, J. Photoch. Photobio. B. 238 (2023) 112622.
[33] L.M. Morton, T.J. Phillips, Wound healing and treating wounds: differential diagnosis and evaluation of chronic wounds, J. Am. Acad. Dermatol. 74 (2016) 589–606.
[34] R.N. Dong, B.L. Guo, Smart wound dressings for wound healing, Nano Today 41 (2021) 101290.
[35] X.Y. Lyu, F.Y. Cui, H. Zhou, B. Cao, X.L. Zhang, M.H. Cai, S.L. Yang, B.Y. Sun, G. Li, 3D co-culture of macrophages and fibroblasts in a sessile drop array for unveiling the role of macrophages in skin wound-healing, Biosens. Bioelectron. 225 (2023) 115111.
[36] J.T. Bjerrum, Y.L. Wang, J.T. Zhang, L.B. Riis, O.H. Nielsen, J.B. Seidelin, Lipidomic trajectories characterize delayed mucosal wound healing in quiescent ulcerative colitis and identify potential novel therapeutic targets, Int. J. Biol. Sci. 18 (5) (2022) 1813–1828.
[37] Y. Morita, T. Sakaguchi, K. Ikegami, N. Goto-Inoue, T. Hayasaka, V.T. Hang, H. Tanaka, T. Harada, Y. Shibasaki, A. Suzuki, K. Fukumoto, K. Inaba, M. Murakami, M. Setou, H. Konno, Lysophosphatidylcholine acyltransferase 1 altered phospholipid composition and regulated hepatoma progression, J. Hepatol. 59 (2) (2013) 292–299.
[38] J.C. Sun, H.Q. Zhao, C.A. Shen, S.Y. Li, W. Zhang, J.L. Ma, Z.S. Li, M. Zhang, J. Q. Yang, Tideglusib promotes wound healing in aged skin by activating PI3K/Akt pathway, Stem Cell Res. Ther. 13 (2022) 269.
[39] M.O. Freitas, A.P.R. Fonseca, M.T. Aguiar, C.C. Dias, R.L. Avelar, F.B. Sousa, A.P.N. N. Alves, S.G.B. Paulo, Tumor necrosis factor alpha (TNF-alpha) blockage reduces acute inflammation and delayed wound healing in oral ulcer of rats, Inflammopharmacology 30 (2022) 1781–1798.
[40] A.A. Shefa, M. Park, J.G. Gwon, B.T. Lee, Alpha tocopherol-nanocellulose loaded alginate membranes and Pluronic hydrogels for diabetic wound healing, Mater. Design 224 (2022) 111404.
[41] A.J. Young, G.L. Lowe, Carotenoids-antioxidant properties, Antioxidants 7 (2) (2018) 28.
[42] L. Paoletti, P. Domizi, H. Marcucci, A. Montaner, D. Krapf, G. Salvador, C. Banchio, Lysophosphatidylcholine drives neuroblast cell fate, Mol. Neurobiol. 53 (9) (2016) 6316–6331.
[43] RD. Semba Perspective, The potential role of circulating lysophosphatidylcholine in neuroprotection against Alzheimer disease, Adv. Nutr. 11 (4) (2020) 760–772.
[44] Z. Qiu, X. Chen, T. Geng, Z.Z. Wan, Q. Lu, L. Li, K. Zhu, X.N. Zhang, Y.J. Liu, X. Y. Lin, L.K. Chen, Z.L. Shan, L.G. Liu, A. Pan, G. Liu, Associations of serum carotenoids with risk of cardiovascular mortality among individuals with type 2 diabetes: results from NHANES, Diabetes Care 45 (6) (2022) 1453–1461.
[45] E. Schilling, Ronald Weiss, A. Grahnert, M. Bitar, U. Sack, S. Hauschildt, Molecular mechanism of LPS-induced TNF-alpha biosynthesis in polarized human macrophages, Mol. Immunol. 93 (2018) 206–215.
[46] S. Chiba, T. Hisamatsu, H. Suzuki, K. Mori, M. Kitazume, K. Shimamura, S. Mizuno, N. Nakamoto, K. Matsuoka, M. Naganuma, T. Kanai, Glycolysis regulates LPS-induced cytokine production in M2 polarized human macrophages, Immunol. Lett. 183 (2017) 17–23.
[47] F.F. Lv, H.F. Liu, G.Q. Zhao, E.M. Zhao, H.Y. Yan, R.J. Che, X.J. Yang, X.H. Zhou, J. C. Zhang, X.J. Liang, Z.H. Li, Therapeutic exosomal vaccine for enhanced cancer immunotherapy by mediating tumor microenvironment, iScience 25 (1) (2022) 103639.

[48] P. Stoitzner, L.K. Green, J.Y. Jung, K.M. Price, H. Atarea, B. Kivell, F. Ronchese, Inefficient presentation of tumor-derived antigen by tumor-infiltrating dendritic cells, Cancer Immunol. Immunother. 57 (2008) 1665–1673.
[49] J.S. Klarquist, E.M. Janssen, Melanoma-infiltrating dendritic cells: limitations and opportunities of mouse models, OncoImmunology 1 (2012) 1584–1593.
[50] M. Rescigno, F. Granucci, P. Ricciardi-Castagnoli, Molecular events of bacterial-induced maturation of dendritic cells, J. Clin. Immunol. 20 (2000) 161–166.
[51] T. Vesikari, S. Esposito, R. Prymula, E. Ypma, I. Kohl, D. Toneatto, P. Dull, A. Kimura, Immunogenicity and safety of an investigational multicomponent, recombinant, meningococcal serogroup B vaccine (4CMenB) administered concomitantly with routine infant and child vaccinations: results of two randomised trials, Lancet 381 (9869) (2013) 825–835.
[52] J. Wo, Z.Y. Lv, J.N. Sun, H. Tang, N. Qi, B.C. Ye, Engineering probiotic-derived outer membrane vesicles as functional vaccine carriers to enhance immunity against SARS-CoV-2, iScience 26 (1) (2023) 105772.